Stability of a Multilateral Junction: Experimental Results and Numerical Modeling

P. Papanastasiou, Schlumberger Cambridge Research; **M. Sibai,** U. of Lille; **J. Heiland,** Schlumberger Cambridge Research; **J.-F. Shao**, U. of Lille; **J. Cook,** Schlumberger Cambridge Research; **D. Fourmaintraux,** and **A. Onaisi,** TotalFinaElf; **B. Jeffryes,** Schlumberger Cambridge Research; and **P. Charlez,** TotalFinaElf

Summary

We studied the stability of multilateral (ML) junctions in a combined experimental and numerical modeling program. The experiments were carried out in a true triaxial machine on large cubic blocks (40 cm) of weak triassic sandstone with two holes intersecting. Six tests have been performed with two different geometrical configurations and three different stress states. The experimental results are presented and compared with numerical modeling obtained with finite-element software developed for assessing the integrity of rock surrounding an ML junction.

Introduction

Drilling inclined wells through producing strata can greatly improve reservoir drainage and hydrocarbon recovery. The horizontal sections are accessed through multiple inclined wells drilled from a relatively small footprint in many or all directions, something that allows better exploitation of offshore platforms and land rigs that are under economic and environmental restrictions. Drilling inclined and horizontal wells, though, is more difficult and more expensive because of wellbore instabilities. A particular area of concern is the integrity of the rock near an ML junction. The junction is the region in which a second wellbore (lateral) takes off from the main wellbore (parent). In the terminology used for ML junctions, different levels are defined according to whether there is mechanical and/or hydraulic integration between lateral and parent holes. By the ML Levels 1 and 2 definitions, the rock at the junction is not supported mechanically with cemented casing, so the integrity of the rock around the area of two intersecting tubes becomes very important in terms of stability.

We performed physical tests on large cubic blocks (40 cm) with two holes intersecting, in the true triaxial cell of the U. of Lille. The tested rock is weak Triassic sandstone called "Grés des Vosges." Six tests have been performed with two different geometrical configurations (lateral differently oriented with respect to the main bore) and three different stress states (two blocks with a hydrostatic stress state and three blocks with anisotropic stress state). The blocks were loaded to generate breakouts of the borehole wall in various directions. The deformation of the borehole walls and the development of breakouts are monitored in real time with a video camera placed in the main bore. The image is then analyzed by image-processing software. Graphs of the relative diametric decrease (convergence of the borehole wall) in various directions can then be plotted against loading. After testing, the blocks were cut in cross sections perpendicular to the parent-hole axis at different distances from the junction. The experimental technique and results will be presented in the Rock Characterization and Experimental Procedure and the Experimental Results sections, later in this paper.

We compared the experimental results with numerical modeling obtained with software developed for assessing the integrity of rock surrounding an ML junction. The tool was developed using finite-element analysis and a graphical user interface for providing the input data and visualizing the results. The analysis is based on a generalized plane-strain formulation that is carried out in cross sections in succession, perpendicular to the parent-hole axis. We compared the load level at which breakouts are initiated. Results are presented for two different junction geometries and three different loading paths (in isotropic loading, all three applied stresses on the block were the same, and in anisotropic loading, two of the applied stresses were the same, and the third stress had a different magnitude). The results, based on the elastic/brittle analysis, qualitatively reproduce those obtained during the experimental tests.

The developed tool will be useful to drilling engineers to decide in which formation, in which azimuth, and with which deviation to drill a stable lateral. The completion engineer can use the tool to decide (a) where to place a stable junction (e.g., in the reservoir or in the overburden), (b) what level of ML junction is needed (mechanically supported or not), and (c) if the junction is drilled in the reservoir section, at which drawdown and depletion pressures it may become unstable.

In other related work, Aadnoy and Edland (1999) considered the stability of two adjacent holes using an analytical solution derived earlier by Savin (1961). This solution is valid for parallel holes embedded in an isotropic stress field. Willson et al. (2000) used a 3D finite-element elastoplastic analysis for assessing the stability of ML junctions. In our approach, we used finite-element analysis carried out in planes perpendicular to the parent-hole axis. The analysis is exact for a single inclined wellbore, and we do not expect large deviations, as long as the build angle of the lateral is small, which is the case in field conditions.

In the next section, we present the experimental procedure and rock characterization. We then present experimental results for different geometries and loading conditions in the Experimental Results section. In the Finite-Element Tool section, we summarize the finite-element modeling and then apply the model to analyze and compare the predictions with the experimental observations in the Comparison of the Experimental Results with Numerical Modeling section. Comparisons are presented for isotropic and anisotropic loading. We also discuss at which direction (with respect to the in-situ stresses) a drilled lateral hole will be more stable. Finally, the main conclusions are drawn in the Conclusions section.

Rock Characterization and Experimental Procedure

The physical experiments to understand the stability of an ML junction and assess the software tool were carried out in the true triaxial machine at Lille U. (Sibai and Shao 2001) The tested blocks are cubes of 40-cm sides. Tests were carried out for cases of parent and lateral holes drilled at different orientations and for different applied-stress paths. The tested rock is weak sandstone called Gres des Vosges. Specially designed visualization equipment was used to monitor the deformation and failure of the holes during the application of the load. At the end of the tests, the blocks were cut in planes perpendicular to the parent-hole axis to observe the integrity of the rock at different distances from the junction. Extended reports on the experimental procedure and rock

This paper (SPE 78212) was first presented at the This paper was prepared for presentation at the 2002 SPE/ISRM Rock Mechanics Conference, Irving, Texas, 20–23 October, and revised for publication. Original manuscript received for review 28 July 2004. Revised manuscript received 27 October 2005. Paper peer approved 10 November 2005.

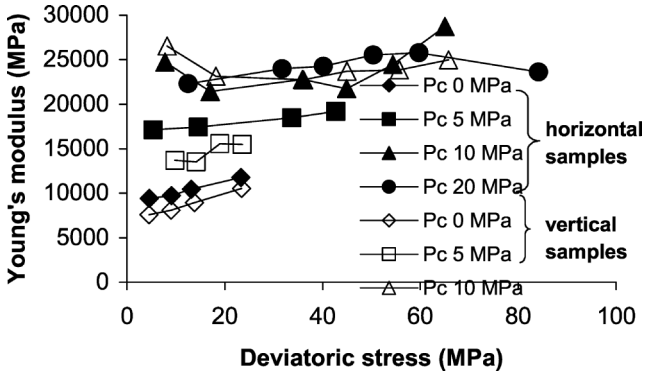

Fig. 1—Elastic modulus vs. applied deviatoric stress in triaxial tests.

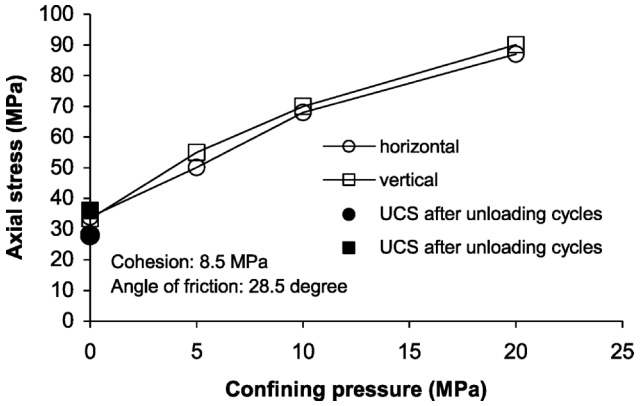

Fig. 2—Peak stress vs. confining pressure in triaxial tests.

characterization can be found in Sibai and Shao (2001). This information was summarized within this paper.

Fig. 1 shows the variation of the elastic modulus vs. applied deviatoric stress obtained from standard triaxial tests with different confining pressure. We observed that there is a significant increase with increasing confining pressure, but only small variations with applied load in each test of constant confining pressure. In addition, there is no strong variation for confining pressures higher than 10 MPa. In the simulations, we used the average saturation value of 22.5 GPa.

The triaxial compression tests showed a slight anisotropy with strength difference, approximately 2 to 5 MPa; horizontal samples are the weaker. Uniaxial compression tests, with loading/unloading cycles, showed a degree of strength anisotropy, with vertical uniaxial compressive strength (UCS) = 36 MPa and horizontal UCS = 28 MPa. **Fig. 2** shows that there is almost a linear variation of peak stress with confining pressure. The estimated Mohr-Coulomb parameters are 8.5 MPa for the cohesion and 28.5° for the friction angle.

Fig. 3 shows the geometrical configuration of the true triaxial tests. The parent hole has a diameter of 37 mm and was drilled through the center of the block. The lateral hole has a diameter of 31 mm and was drilled with 22.5° inclination from the parent hole, but with different orientation in (a) and (b), with respect to the in-situ stresses.

Six experiments have been conducted; five of these were experiments with a lateral borehole, and one experiment was done on a single borehole. The blocks were carefully inspected to verify that they were relatively uniform and that no microcracks or fractures existed that could skew the results, thereby hampering the comparison between the different experiments. **Fig. 4** shows the different geometries of the blocks and the stress conditions under which the six experiments were carried out. The symbols σ_H, σ_h, and σ_V refer to the stress directions applied by the triaxial machine on the samples. σ_V is oriented parallel to the axis of the main borehole and, during the experiments with anisotropic stress conditions, its value was always 0.6 times the maximum stress.

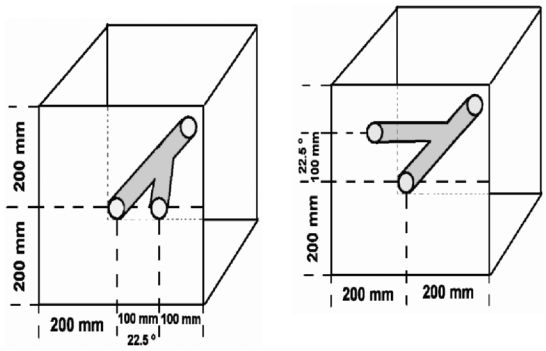

Fig. 3—Geometrical configurations of the tests.

The numbers give the multiplier of the stresses acting on the rocks; σ_V equals 0.6 times the maximum stress for all anisotropic experiments (Experiments 3 through 6). During the experiments, the stresses were increased in steps of 3 MPa (for that stress with the multiplier 1), and when each loading step was reached, the actual value was recorded through a microphone on the videotape. In the following section, σ_{max} denotes the value of the stress, which has the multiplier 1, and σ_{min} denotes the value of the two stresses with multiplier 0.6.

Experimental Results

During the experiments, the main borehole and parts of the junction were observed using an endoscopic camera and a light guide, which projects a ring of light on the borehole wall. From the recorded videotapes, the borehole deformation and the stresses at which failure occurs can be determined. The position of the camera varied during the experiments: the camera either was looking into the lateral borehole (Experiments 1 and 3) or was positioned behind the junction (Experiments 2, 4, and 5), so that the lateral borehole was seen as an elliptical shadow on the wall of the main borehole. This means that in the first case, it was not possible to observe the onset of failure of the junction (i.e., the material, or the pillar, between the two boreholes).

Comparison of Experiments 3 and 5 shows that the junction with the lateral hole drilled parallel to the maximum stress (Experiment 5) is more stable than when the lateral is drilled perpendicular to the maximum stress (Experiment 3). The onset of failure in the main borehole is at 39 MPa in Experiment 5, compared to 30 MPa in Experiment 3. (In Experiment 3, the lighting conditions were very unfavorable, so that the onset of failure could even be earlier, at approximately 27 MPa.) The onset of failure of the

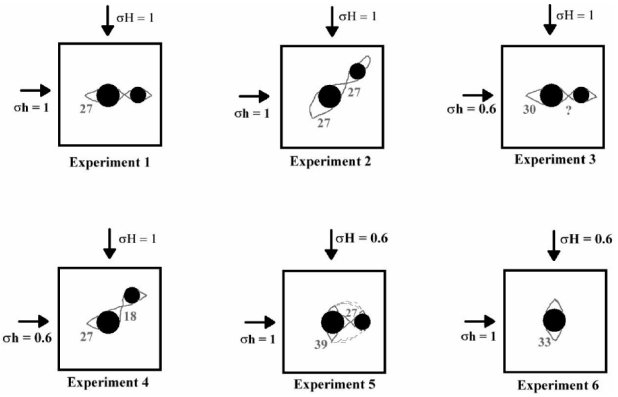

Fig. 4—Geometries and stress conditions of the six experiments. Sketch of the breakout shapes observed after the experiments. The numbers in the blocks give the maximum stresses (MPa) at which the failure of the main borehole and the junction started.

junction took place at 27 MPa in Experiment 5. In Experiment 3, this was not possible to determine, but it certainly took place at lower stresses than in Experiment 5.

The failure stress and mode in Experiment 2 are very similar to those in Experiment 1, as expected from the isotropic stress. The junction of a lateral drilled at 45° to the principal-stress directions and subjected to anisotropic stresses fails at much lower stresses than under isotropic-stress conditions. How this result compares to Experiment 3 cannot be determined, because in that experiment, the junction was not visible during the test.

The failure stress of the single hole (Experiment 6) is relatively low, especially compared to Experiment 5; however, the onset of failure in the single hole is still higher than the highest strength of the junction. The lower strength in the single-hole experiment may also be caused by differences in the rock samples.

Another interesting finding is that under isotropic-stress conditions, the junction fails at the same stress level as the main borehole, as was observed in Experiments 1 and 2. On the contrary, under anisotropic-stress conditions, it was always observed that the junction (that is the pillar between the two boreholes) fails first, and the failure of the main borehole starts at a higher stress.

Single, digital snapshots were taken from the videotapes at each load step, or when a new failure had occurred, and analyzed for the deformation of the main borehole. This analysis was done using an image-analysis software package developed by the U.S. Natl. Inst. for Health. The reduction of the borehole size was determined either by measuring the length of single diameters (Experiment 1) or by measuring the reduction of the area (Experiments 2 through 6) of the light ring projected on the borehole wall. The results of this analysis are shown in **Fig. 5,** in which the borehole deformation (that is the reduction of the borehole size compared to the initial borehole size) is plotted against the maximum stress (σ_{max}) applied to the rock sample.

Depending on the lighting conditions during the experiments, the beginning of failure may be seen very early by a change of the roughness of the borehole wall, which develops into a fracture when the stress is further increased (this roughness can be seen in Fig. 7 at the bottom of the main borehole and in Fig. 10—the failure in this area is fully developed). In Fig. 5, the onset of failure, shown by the arrows, is when the first fracture is clearly visible. The failure of the junction normally starts with small pieces of rock falling off from the edge between the two boreholes. This corresponds to the arrows denoting failure of the junction in Fig. 5. Once the junction starts failing, a fracture tends to grow along the wall of the main borehole, accompanied by larger pieces of loose rock that fall down.

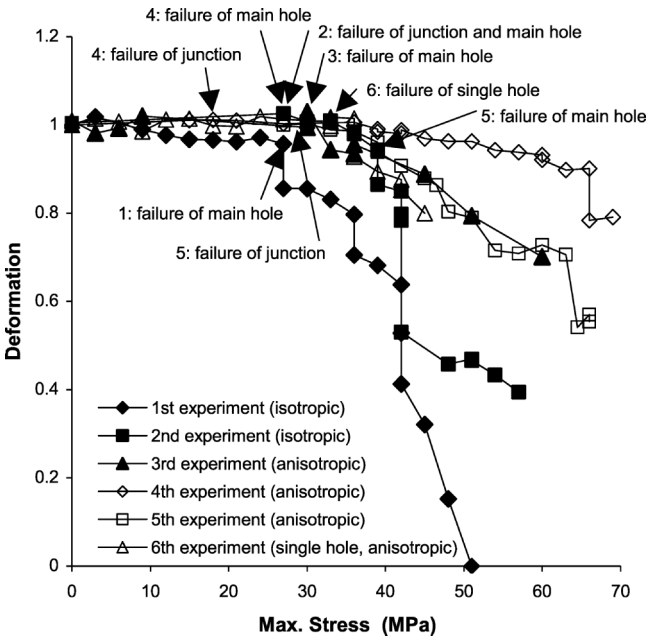

Fig. 5—Deformation of the main borehole vs. maximum stress applied on the rock samples. The arrows show the points at which failure of the junction and/or main borehole started.

The amount of deformation that occurred in each experiment should not be taken as an absolute measure for any further analysis because the image analysis is not able to give accurate numbers. The diagram in Fig. 5 is only meant to give an impression of what happens inside a borehole while it is failing. The analysis of deformation in the experiments is difficult because the blocks were oriented inside the triaxial machine in such a way that the main borehole was lying horizontally. Because of gravity, the failed material at the "roof" of the borehole tends to fall down and accumulate at the "floor" of the borehole. The deformation obtained from image analysis would be interpreted as an increase in borehole radius at the top of the borehole and a decrease at the bottom.

In the deformation analysis of Experiment 1, several radii were measured, and the one plotted in Fig. 5 is located in the main borehole, opposite the junction with the lateral. The deformation was so high that the borehole wall touched the light guide in the end. In all other experiments, the area marked by the light guide in the main bore was measured for deformation analysis. This means that the deformation is averaged over the whole borehole area. The stresses at which the junction and the main borehole started to fail during the experiments are summarized in **Table 1.**

Finite-Element Tool

2D plane-strain solutions can be applied to analyze the stability of ML junctions when the wellbore axis is nearly parallel to the direction of one of the in-situ stresses. For example, this is very often the case for a vertical or a horizontal parent wellbore. In the general case of an inclined parent hole, however, a more elaborate analysis is required because the problem is 3D and all components of the stress tensor are involved. Nevertheless, the construction of engineering models can be simplified and computational time can be reduced significantly by simplifying the geometry, taking into account the following two points:

- The analysis can be carried out in a local coordinate system the z-axis of which is parallel to the parent-hole axis. The x-axis is chosen to be parallel to the lower-most radial direction of the parent wellbore, and the y-axis is horizontal. The build angle between the lateral hole and parent hole is usually small, so the axis of the lateral is nearly close to the z-axis. Then, the in-situ stresses in this local frame consist of three normal and three shear components. To model wellbores of different orientations, only the decomposition of the in-situ stress field in the local frame needs to be changed. Thus, only one finite-element mesh is required with a change of the applied stresses, according to the wellbore orientation. The transformed in-situ stresses are applied in the form of an initial stress condition.
- It is expected that there is no significant variation in the deformation of the cross sections perpendicular to the wellbore's axis caused by the in-situ stresses. The differences in the deformation of the cross sections along the z-axis are mainly caused by the changes of the in-plane geometries. The nodal displacements of the different cross sections can be decoupled, resulting in local displacements independent of the position of the node along the parent wellbore axis. Thus, no significant variation of the displacement field (u_x, u_y, u_z) is expected, parallel to the hole z-axis.
- These conditions can be easily implemented in a 2D finite-element code in which the third equilibrium equation (i.e., in the z-direction) replaces the plane-strain condition. Thus, the solution domain is a plane perpendicular to the hole axis, with the three components of the displacement being the primary unknowns. This formulation allows out-of-plane warping of a thin layer without change of its thickness.

The data are given through a graphical interface, shown in **Fig. 6** for a particular example. The data required to define the geometry are the radii of the holes, the inclination and azimuth of the parent hole, build angle between lateral and parent holes, and the position of the lateral with respect to the lowest point on the parent hole. The rock parameters are defined by the elastic modulus and

TABLE 1—EXPERIMENTAL RESULTS

Experiment Number		Failure of Junction				Failure of Main Borehole			
		σ_{Max}, MPa	σ_{min}, MPa	σ_M $(\sigma_1+\sigma_2+\sigma_3)/3$, MPa	σ_D $(\sigma_{Max}-\sigma_{min})$, MPa	σ_{Max}, MPa	σ_{min}, MPa	σ_M $(\sigma_1+\sigma_2+\sigma_3)/3$, MPa	σ_D $(\sigma_{Max}-\sigma_{min})$, MPa
6	Single hole, anisotropic stress	—	—	—	—	33	19.8	24.2	13.2
1 and 2	Isotropic stress	27	—	27	—	27	—	27	—
3	Both holes along σ_{min}			(junction not visible)		30	18	22	12
5	Both holes along σ_{Max}	27	16.2	19.8	10.8	39	23.4	28.6	15.6
4	Lateral 45° to main stress axis	18	10.8	13.2	7.2	27	16.2	19.8	10.8

Poisson's ratio, the friction angle, and the rock strength (UCS). The input stresses in the model are the vertical stress and the two horizontal stresses, the reservoir pressure, and the well pressure. The direction of the maximum horizontal stress with respect to North is also needed. Finally, a Biot constant is needed to define the relation between total and effective in-situ stresses.

Once the data are provided, the interface shows the actual geometry and the chosen plane perpendicular to hole axis where the stress analysis will be carried out. The cross section of this plane with the holes is shown in the lower graph of Fig. 6. After all data are defined, the finite-element routines automatically define the mesh and carry out the analysis. The results are processed and shown in the lower graph. Contours can be provided either for the maximum principal stress or for a yield factor that shows the area where the stresses, calculated from the elastic analysis, exceed the Mohr-Coulomb yield criterion.

Comparison of the Experimental Results With the Numerical Modeling

The model predictions in this section are based on linear elasticity; therefore, we expect that the prediction of the stress level needed to induce failure will be conservative. Nevertheless, we will examine whether the model can correctly predict which areas are prone to fail. As we will see later, the failure-load predictions can be improved with the introduction of the boost factors.

The first two tests were run under isotropic loading, using the block geometries depicted in Fig. 4. Although the geometry is different for each test, because the applied-stress field is isotropic, the obtained experimental results are similar, as was anticipated. For this reason, in this section we will model the two tests using the same data.

During testing, the three applied stresses on the sides of the blocks were increased equally. In the following computations, we will compare the images, showing the integrity of the rock around the junction with the model's prediction at different levels of loading. Failure around the holes in both tests was observed after the applied isotropic stresses reached the value of 27 MPa. In Test 1, the position of the camera prevented the observation of any signs of failure around the junction, as in Test 2 depicted in **Fig. 7.** In both tests, there were signs of failure around the parent hole at 27 MPa pressure.

The model predictions are shown in **Figs. 8 and 9** for comparison with the experiments. Fig. 8 shows that the model predicts maximum compressive stress around the junction area. This prediction is in agreement with Test 2, which allows such an observation (Fig. 7). According to the images from both tests, the next sections close to failure are some areas around the parent and lateral holes (failure around the lateral cannot be observed because of the position of the camera).

In Fig. 9, we plot the corresponding yield factors for two cross sections. The area that yields, and eventually fails, is the area where the yield factor has a value greater than 1. The yield factor was calculated here on the basis of elastic analysis; hence, values greater than 1 are possible. In reality, once yielding starts, the stresses will decrease in the yielded area and increase further internally, pulling a greater area into yield. Although the yielded area appears to be nearly circular, the distribution of the maximum compressive stress is nearly anisotropic, with the maximum value in the area surrounding the long axis of the holes (Fig. 8).

Fig. 10 shows extensive signs of failure around the junction at higher loads observed in the two tests. As we expect with further increase of the stresses, the failed area around the hole has spread in the interior.

The final applied stresses on the first block were 63 MPa. After testing, a plastic pipe was placed in the holes, and the areas in the annulus were filled with epoxy to keep the failed areas in place **(Fig. 11).** The block was cut in cross sections parallel to the parent-hole axis at different distances from the junction. We compared the

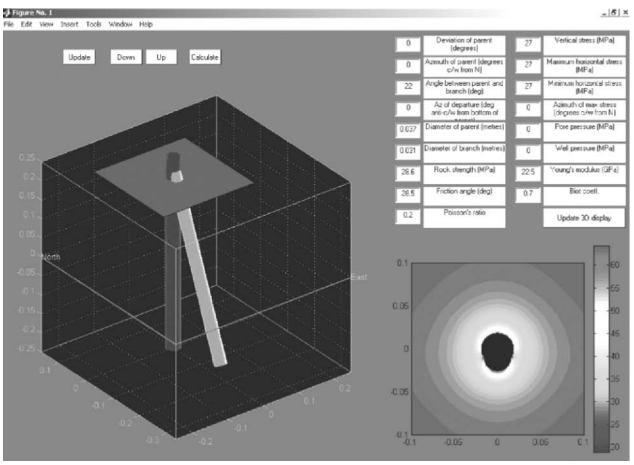

Fig. 6—User interface of multilateral stability tool.

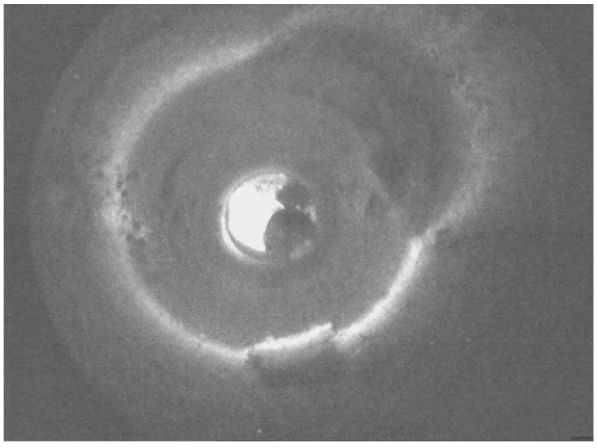

Fig. 7—Failed area around the ML junction for 27 MPa stresses in Experiment 2.

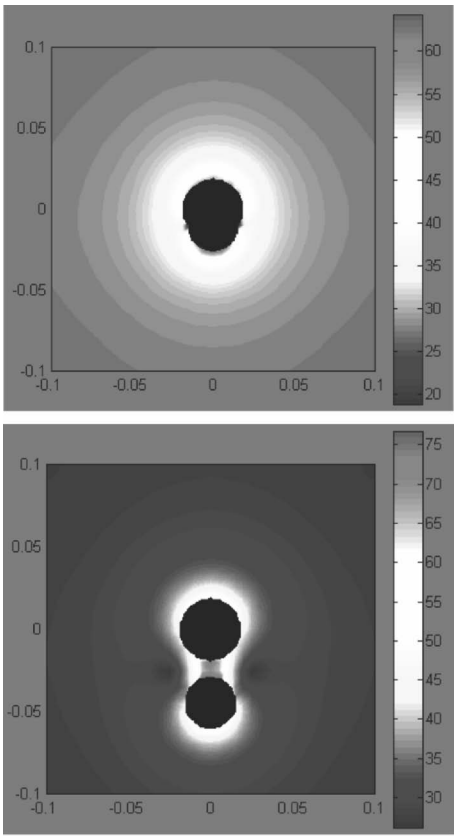

Fig. 8—Model predictions of maximum compressive stress at 27 MPa stresses at two different points along the junction.

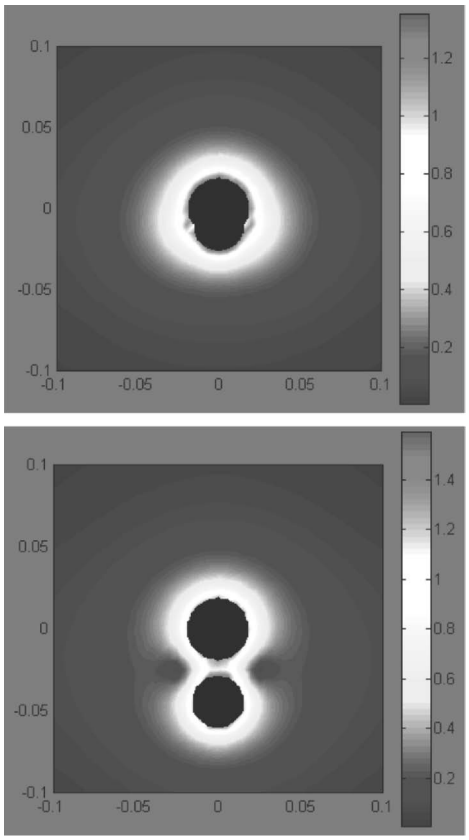

Fig. 9—Model predictions of yielded area at 27 MPa stresses at two different points along the junction.

images of these cross sections with the model predictions in **Fig. 12.** The predicted failed area, based on the maximum compressive stress, is in agreement with the failed area observed in the experiment. In all the cases, the predicted failed region is the area between the two holes and the area across the axis that connects the two holes. Recall that according to Test 2, the load level at which failure initiated was approximately 27 MPa.

The third experiment was run under anisotropic loading. The tested block geometry was the same as in Block 1 (Fig. 3, left). The minimum horizontal stress was kept at 0.6 times the maximum horizontal stress. The vertical stress (parallel to the parent-hole axis) was maintained equal to the minimum horizontal stress. Failure was observed around the parent hole after the stresses reached the level of $\sigma_V = \sigma_h = 18$ MPa, $\sigma_H = 30$ MPa (**Fig. 13,** top). As we will see in the next test, the junction might have failed at lower pressures, but it is not possible to see it in Test 3 because of the position of the camera. The model predictions are shown in **Fig. 14,** top. The stress concentration around the failed area is slightly higher than the stress concentration in the isotropic tests.

The fourth experiment was also run under anisotropic loading, but with the second block geometry (Fig. 3, right). As in the third test, the minimum horizontal stress was kept at 0.6 times the maximum horizontal stress, and the vertical stress (parallel to the parent-hole axis) was maintained equal to the minimum horizontal stress. Failure was observed right at the junction after the stresses have reached the level of $\sigma_V = \sigma_h = 12.6$ MPa, $\sigma_H = 21$ MPa (**Fig. 15a,** top). In this test, the lighting of the borehole was much better, so one can really see the failed areas first, right at the junction and then around the parent hole. Compared to the failure load in Test 3, failure in Test 4 was initiated at lower loading. It is possible that in the third test, failure was initiated at a lower load level, but it was difficult to view it because of poor light and the position of the camera. The model predictions are shown in **Fig. 16.** Further comparisons were made for higher applied stresses in Figs. 15 and 16, where more areas around the holes have failed. The stress concentration in the failed areas in the fourth test is comparable with the stress concentration of the isotropic test (Fig. 8). We mention here that some discrepancies on the load that initiates failure were observed between the tests; a possible explanation is that it may be difficult to identify the instant at which failure is initiated because of poor lighting and the position of the camera. However, there is

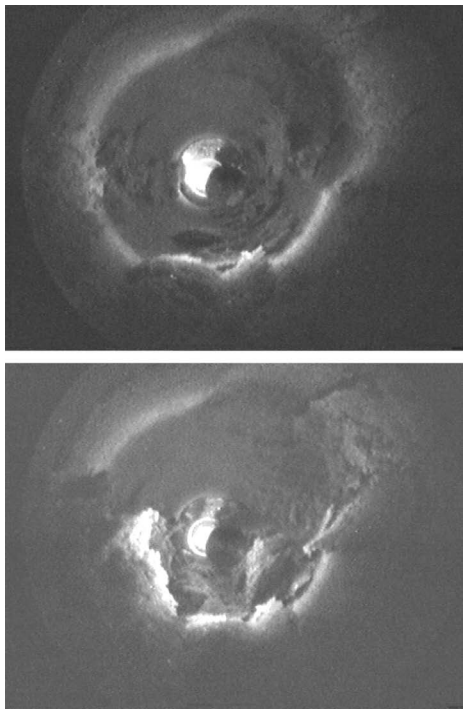

Fig. 10—Failed area in Experiment 1 at 36 MPa (top) and 45 MPa (bottom) applied stresses.

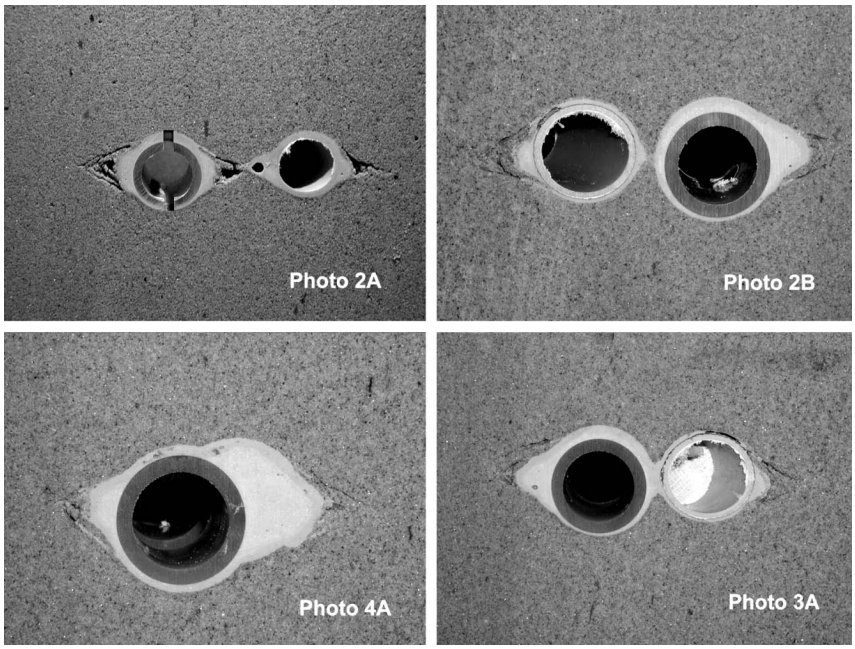

Fig. 11—Cross-sectional images obtained at the end of the Test 1 after the appled stresses reach 63 MPa.

more consistency between the load levels at which the same areas around the hole fail.

In summary, the results of isotropic and anisotropic tests show that failure at the same area is initiated around the same maximum applied stress, 30 MPa (Fig. 4), though elasticity predicts slightly higher stress concentration in the case of anisotropic loading.

It seems that the present model, based on elasticity, indicates which are the most sensitive areas to fail around the junction, but underestimates the load level at which failure initiates. More realistic results could be obtained by incorporating a plasticity-material model, although the tested rock in the physical tests has shown a pronounced elastic/brittle behavior. Alternatively, better quantitative predictions can be obtained by employing a more robust analysis and failure criterion on the basis of the localization of deformation (Papanastasiou and Zervos 2004). From a practical point of view, we suggest using a boost factor for the rock strength, as is done routinely in the case of a single wellbore (Zervos et al. 1998). The boost factor is defined as the ratio of the model-predicted maximum compressive stress near the borehole wall over the UCS of the rock at failure. For example, from the experimental results of Fig. 11 and the corresponding modeling results of Fig. 12, the boost factor = 150/32 = 4.68. In field calculations, failure will assume to take place when the predicted maximum compressive stress exceeds the value 4.68×32 = 150 MPa. Though ex-

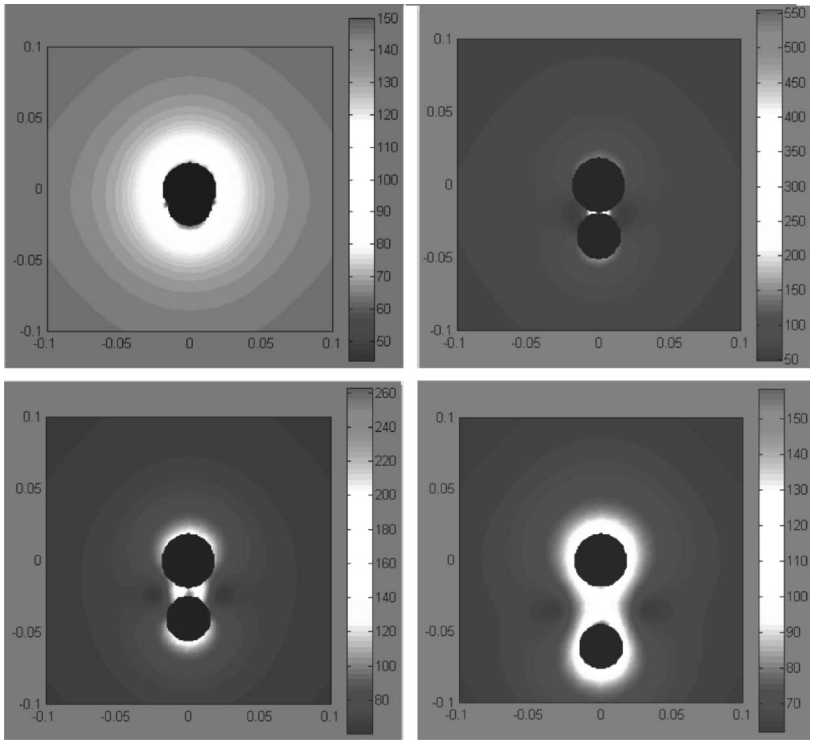

Fig. 12—Predicted maximum compressive stress at different cross sections for 63-MPa applied stresses, to be compared with the images of Fig. 11.

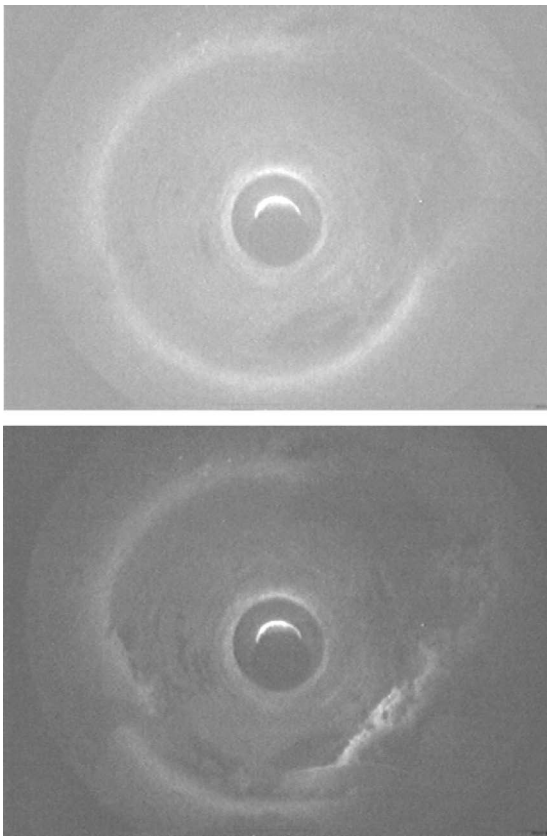

Fig. 13—Image of ML junction in test 3 for $\sigma_V = \sigma_h = 18$ MPa; $\sigma_H = 30$ MPa (top); $\sigma_V = \sigma_h = 21.6$ MPa; and $\sigma_H = 36$ MPa (bottom).

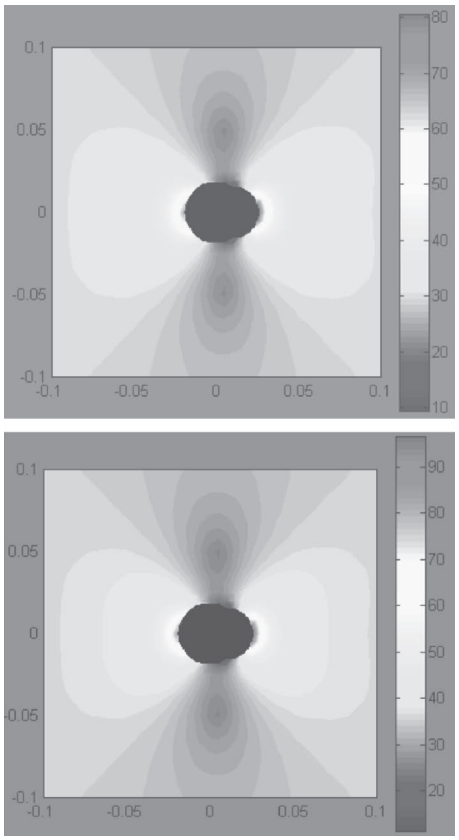

Fig. 14—Predicted maximum compressive stress for $\sigma_V = \sigma_h = 18$ MPa; $\sigma_H = 30$ MPa (top); $\sigma_V = \sigma_h = 21.6$ MPa; and $\sigma_H = 36$ MPa (bottom).

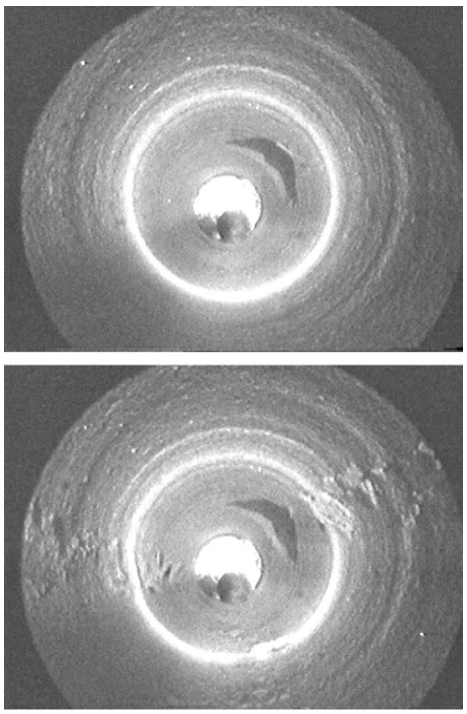

Fig. 15—Experiment 4, image of ML junction for $\sigma_V = \sigma_h = 12.6$ MPa; $\sigma_H = 21$ MPa (top); $\sigma_V = \sigma_h = 23.4$ MPa; and $\sigma_H = 39$ MPa (bottom).

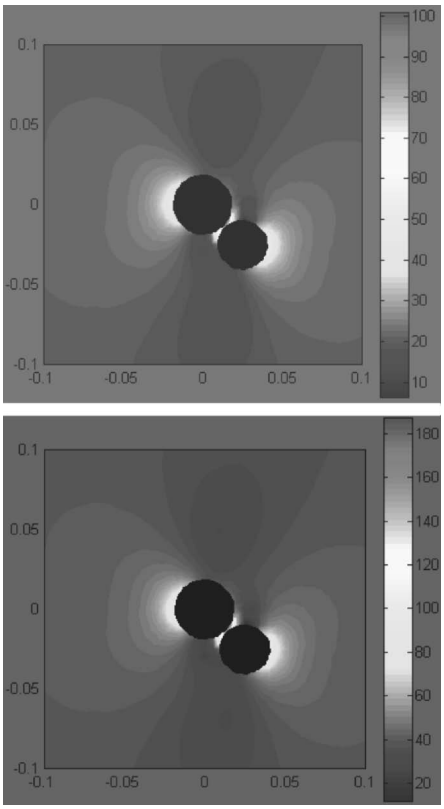

Fig. 16—Predicted maximum compressive stress ML for $\sigma_V = \sigma_h = 12.6$ MPa; $\sigma_H = 21$ MPa (top), and $\sigma_V = \sigma_h = 23.4$ MPa; $\sigma_H = 39$ MPa (bottom).

perimental results on hollow-cylinder tests are rarely available, the boost factor can be extracted from the experience gained on wellbore stability during drilling of the parent hole and subsequently used in the ML stability analysis. Borehole images from the parent hole can be analyzed to derive a boost factor to be used in the stability analysis of a junction. For example, if no signs of breakouts were observed during drilling of the parent hole, the boost factor shall be higher than the ratio of the predicted maximum compressive stress over the rock UCS.

Conclusions

We studied the stability of a ML junction in a combined experimental and numerical modeling program. The experiments were carried out in a true triaxial machine on large cubic blocks (40 cm) of weak Triassic sandstone with two holes intersecting. We presented the results of six tests performed with three different geometrical configurations and three different stress states. Images of the junction were obtained during testing using specially designed visualization equipment and from cross-sectional cuts at the end of the experiments.

We have presented a software tool developed to assess the integrity of the rock near an ML junction. The tool was based on finite-element analysis that is carried out in planes perpendicular to the parent-hole axis. We used the tool to analyze and compare the predictions with experiments. The software tool predicts reasonably well the area around the holes that is prone to failure. However, it underestimates the load level at which failure will initiate. It seems that for field applications, as in the case of a single wellbore, a boost factor for the rock strength is needed to get more realistic failure stresses. One suggestion is to use a boost factor derived from the experience gained during drilling of the parent wellbore.

We have also investigated the direction of a more stable lateral with respect to the in-situ stresses. We found that the most stable direction for a lateral to be drilled is parallel to the maximum in-situ stress.

Nomenclature

u_x = displacement along the x axis
u_y = displacement along the y axis
u_z = displacement along the z axis
σ_h = minimum horizontal stress
σ_H = maximum horizontal stress
σ_{Max} = maximum applied stress
σ_{min} = minimum applied stress
σ_V = vertical stress

Acknowledgment

Part of this research was funded by the French government organization COPREP.

Reference

Aadnøy, B.S. and Edland, C. 1999. Borehole Stability of Multilateral Junctions. Paper SPE 56757 presented at the SPE Annual Technical Conference and Exhibition, Houston, 3–6 October.

Papanastasiou, P. and Zervos, A. 2004. Wellbore Stability Analysis: From Linear Elasticity to Post-Bifurcation Modeling. *Intl. J. of Geomech. (ASCE)* **4** (1) 2–12.

Savin, G.N. 1961. *Stress Concentration Around Holes.* Oxford, England: Intl. Ser. Monogr. Aeronautics and Astronautics, Pergamon, **1**, 430.

Sibai, M. and Shao, J.-F. 2001. Determination des Caracteristiques d'un Gres des Vosges Pour l'Etude de la Stabilite de la Jonction Multilaterale d'un Puits Petrolier. Laboratoire de Mecaniquie de Lille, U. de Sciences et Technologies de Lille.

Willson, S.M., Dowson, S.L., and Plischke, B. 1999. Numerical Simulation of the Stability of Multilateral Well Junctions. Paper presented at the 9th ISRM Intl. Congress Symposium, Paris.

Zervos, A., Papanastasiou, P., and Cook, J. 1998. Elastoplastic Finite Element Analysis of Inclined Wellbores. Paper SPE/ISRM 47322 presented at the SPE/ISRM Rock Mechanics in Petroleum Engineering, Trondheim, Norway, 8–10 July.

Panos Papanastasiou is currently Associate Professor and Head of the Dept. of Civil and Environmental Engineering at the U. of Cyprus. He worked as Research Scientist and Principal Research Scientist in Schlumberger Cambridge Research from 1991 to 2002, in the areas of geomechanics, hydraulic fracturing, wellbore stability, sand production and control, and reservoir geomechanics. He received his first degree from NTU of Athens and MSc and PhD degrees from the U. of Minnesota, all in civil engineering. **Malek Sibai** has been the Research Engineer in the laboratory of mechanics at the U. of Lille since 1990. He received an MS degree in fluid mechanics from the U. of Poitiers, France, and a PhD degree in civil engineering from the U. of Lille. **Juliane Heiland** has been the Senior Engineer in Schlumberger Reservoir Completions at Rosharon, Texas, since 2004. She worked as Research Assistant at the Academy of Sciences of the Czech Republic from 1994 to 1997, as a postdoctoral researcher at the GeoForschungszentrum Potsdam from 1998 to 2001, and as a senior research scientist in the geomechanics group at Schlumberger Cambridge Research from 2001 to 2004. Heiland holds a Diplom-Geologe in applied geology from the Technical U., Munich, and a PhD degree in applied geology from Charles U., Prague. **J.-F. Shao** is Professor in the Dept. of Civil Engineering and Head of the geomechanics research group at the U. of Lille. He has been working for more than 15 years on laboratory investigation and numerical modeling for thermohydromechanical and chemical coupling in geomechanics. Shao holds a doctoral degree from the U. de Sciences et Technologies de Lille. **John Cook** is a Scientific Adviser at Schlumberger's research center in Cambridge, England. He has worked for Schlumberger for 22 years, mainly in the areas of geomechanics, wellbore instability control, sand production and control, and drilling optimization. He holds an MA degree in natural sciences and a PhD in physics, both from the U. of Cambridge. **Dominique Fourmaintraux** is Senior Geomechanics Adviser at Total E&P, Pau, France. After working for 15 years in civil engineering projects, he joined Elf Aquitaine E&P to organize the Rock Mechanics Laboratory in the Pau Technical Centre. He worked in the Total E&P Drilling and Operations Div., and he is now involved within HSE evaluation of underground storage, injections, or sequestration (of gas or others) during exploitation (short term) and abandonment (long term). **Atef Onaisi** is Head of Geomechanics Services for Total E&P, Pau. He worked 7 years as research engineer in rock mechanics at IFP. He has wide experience in rock mechanics applied to drilling, reservoir engineering, and geology. He received his first degree in civil engineering from the U. of Beirut in Lebanon and a PhD degree in soil and rock mechanics from Ecole Centrale of Paris. **Benjamin Jeffryes** is currently a scientific adviser with Schlumberger Oilfield Research in Cambridge, England. Following post-doctoral work at the Max Planck Inst. for astrophysics in Garching, Germany, he spent 3 years working in acoustics consultancy before joining Schlumberger research in 1990. Jeffryes holds a BSc degree in mathematical physics from the U. of Sussex and a PhD degree in mathematics from the U. of Oxford. **Philippe Charlez** is currently Director of Bloc 3 for Total in Angola. He joined Total in 1982, where he worked as Rock Mechanics Expert between 1988 and 1996, as Senior Drilling Engineer in North Sea from 1996 to 1998, and as R&D Program Manager in charge of drilling and completion, after the merge with Elf, from 1999 to 2003. Charlez holds a degree in mining engineering from Ecole des Mines de Mons, Belgium, and a PhD degree from Inst. de Physique du Globe de Paris.